The Astrophysical Journal Letters, 724:L34–L38, 2010 November 20 doi:10.1088/2041-8205/724/1/L34

ON THE STABILITY OF NON-FORCE-FREE MAGNETIC EQUILIBRIA IN STARS

V. Duez[1], J. Braithwaite[1], and S. Mathis[2]
[1] Argelander Institut für Astronomie, Universität Bonn, Auf dem Hügel 71, D-53111 Bonn, Germany; vduez@astro.uni-bonn.de
[2] Laboratoire AIM, CEA/DSM-CNRS-Université Paris Diderot, IRFU/SAp Centre de Saclay, F-91191 Gif-sur-Yvette, France
Received 2010 July 23; accepted 2010 September 17; published 2010 October 27

ABSTRACT

The existence of stable magnetic configurations in white dwarfs, neutron stars, and various non-convective stellar regions is now well recognized. It has recently been shown numerically that various families of equilibria, including axisymmetric mixed poloidal–toroidal configurations, are stable. Here we test the stability of an analytically derived non-force-free magnetic equilibrium resulting from an initial relaxation (self-organization) process, using three-dimensional magnetohydrodynamic simulations: the obtained mixed configuration is compared with the dynamical evolution of its purely poloidal and purely toroidal components, both known to be unstable. The mixed equilibrium shows no sign of instability under white noise perturbations. This configuration therefore provides a good description of magnetic equilibrium topology inside non-convective stellar objects and will be useful to initialize magneto-rotational transport in stellar evolution codes and in multi-dimensional magnetohydrodynamic simulations.

Key words: magnetohydrodynamics (MHD) – stars: interiors – stars: magnetic field – stars: neutron – Sun: magnetic topology – white dwarfs

1. INTRODUCTION

Magnetic fields are being detected more and more routinely at the surface of many stars and are responsible for various physical phenomena likely to deeply modify our traditional vision of stellar evolution, especially during their early and late stages. The presence of even a relatively weak magnetic field can have an important impact on the collapse and fragmentation of prestellar cores (Commerçon et al. 2010) as well as influencing the rotation rate of pre-main-sequence stars (see, e.g., Alecian et al. 2008). On the other side of the Hertzsprung–Russell diagram its feedback effects may also play a key role in supernovae and mechanical energy deposition in the interstellar medium, for instance.

Magnetic fields are also an important actor in main-sequence stars. First, we cannot dismiss the possibility of a large-scale magnetic field being responsible for the quasi-uniform rotation behavior in the bulk of the solar radiation zone, as revealed by *p*-modes helioseismology (Eff-Darwich et al. 2008). Second, strong fields (300 G to 30 kG) are observed via the Zeeman effect in some fraction of main-sequence A stars (the Ap stars, see, Aurière et al. 2007) as well as in B stars and in a handful of O stars (Grunhut et al. 2009). The bimodality of rotational velocities observed among Ap versus normal A stars shows the critical effect of magnetic fields on rotation and therefore also on meridional circulation and chemical transport (see Mathis & Zahn 2005). Finally, magnetic white dwarfs display field strengths of 10^4–10^9 G, and neutron stars host fields in the range 10^8–10^{15} G, in both cases detected using several distinct methods.

The large-scale, ordered nature of these fields (often approximately dipolar) and the scaling of their strengths as a function of their host properties (according to the flux conservation scenario) favor a fossil hypothesis, whose origin is not yet elucidated.

Another fundamental question is the topology of these large-scale magnetic fields. To have survived since the star's formation, a field must be stable on a dynamic (Alfvén) timescale. It was suggested by Prendergast (1956) that a stellar magnetic field in stable axisymmetric equilibrium must contain both poloidal (meridional) and toroidal (azimuthal) components, since both are unstable on their own (Tayler 1973; Wright 1973; Braithwaite 2006; Bonanno & Urpin 2008b). This was confirmed recently by numerical simulations by Braithwaite & Spruit (2004) and Braithwaite & Nordlund (2006) who showed that an arbitrary initial field evolves on an Alfvén timescale into a stable configuration; axisymmetric mixed poloidal–toroidal fields were found. Once formed, it continues to evolve on longer timescales through diffusive processes such as finite conductivity: the field then moves outward, passing quasi-statically through a series of stable axisymmetric equilibria until it changes eventually to a non-axisymmetric equilibrium. These non-axisymmetric equilibria are described in more detail in Braithwaite (2008).

2. THE RELAXED NON-FORCE-FREE CONFIGURATION

Here, we deal with axisymmetric, non-force-free magnetic configurations (i.e., with a non-zero Lorentz force) in equilibrium inside a conductive fluid. We first restrict ourselves to the non-rotating case, but results also apply to rotating stars where rotation is uniform (Woltjer 1959), which could be the case if magnetic field is strong enough, and where meridional circulation can be neglected (i.e., when the star does not lose angular momentum and has a stationary structure; see Busse 1981; Zahn 1992; Decressin et al. 2009). The more general case including (differential) rotation (and induced meridional circulation) will be studied in a forthcoming work. Several reasons inclined us to focus on non-force-free equilibria instead of force-free ones; let us briefly describe them here. First, Reisenegger (2009) reminds us that no configuration can be force free everywhere. Although "force-free" configurations do exist, they must be confined by some region or boundary layer with non-zero or singular Lorentz force. Discontinuities such as current sheets are unlikely to appear in nature except in a transient manner. Second, non-force-free equilibria have been identified in plasma physics as the result of MHD relaxation (self-organization process involving magnetic reconnections in resistive MHD), e.g., by Montgomery & Phillips (1988) and Shaikh et al. (2008). Third, as shown by Duez & Mathis (2010), this family of

equilibria is a generalization of Taylor states (force-free relaxed equilibria; see Taylor 1974) in a stellar context where the stratification of the medium plays a crucial role.

2.1. The Magnetic Field in MHS Equilibrium

Let us briefly recall the assumptions made in building the semi-analytical model of magnetohydrostatic (MHS) equilibrium described by Duez & Mathis (2010). The axisymmetric magnetic field $\boldsymbol{B}(r,\theta)$ is expressed as a function of a poloidal flux $\Psi(r,\theta)$, a toroidal potential $F(r,\theta)$, and the potential vector $\boldsymbol{A}(r,\theta)$, so that it is divergence free by construction:

$$\boldsymbol{B} = \frac{1}{r\sin\theta}(\boldsymbol{\nabla}\Psi \times \hat{\mathbf{e}}_\varphi + F\,\hat{\mathbf{e}}_\varphi) = \boldsymbol{\nabla}\times\boldsymbol{A}, \quad (1)$$

where in spherical coordinates the poloidal component is in the meridional plane ($\hat{\mathbf{e}}_r$, $\hat{\mathbf{e}}_\theta$) and the toroidal component is along the azimuthal direction ($\hat{\mathbf{e}}_\varphi$). The MHS equation expressing balance between the pressure gradient force, gravity, and the Lorentz force is

$$\mathbf{0} = -\boldsymbol{\nabla}P - \rho\,\boldsymbol{\nabla}V + \frac{1}{\mu_0}(\boldsymbol{\nabla}\times\boldsymbol{B})\times\boldsymbol{B}, \quad (2)$$

where V is the gravitational potential which satisfies the Poisson equation: $\nabla^2 V = 4\pi G\rho$.

2.2. The Non-force-free Barotropic Equilibrium Family

2.2.1. A Variational Approach

Here, we focus on the minimum energy non-force-free MHS equilibrium in stably stratified radiation zones. Given the field strengths in real stars, the ratio of the Lorentz force to gravity is very low: stellar interiors are in a regime where $\beta = P/P_{\rm Mag} \gg 1$, $P_{\rm Mag} = B^2/(2\mu_0)$ being the magnetic pressure. We then identify the two MHD invariants governing the evolution of the reconnection phase, that leads to relaxed states in the non-force-free context: the magnetic helicity $\mathcal{H} = \int_{\mathcal{V}} \boldsymbol{A}\cdot\boldsymbol{B}\mathrm{d}\mathcal{V}$ and the mass encompassed in poloidal magnetic surfaces $M_\Psi = \int_{\mathcal{V}} \Psi\,\rho\,\mathrm{d}\mathcal{V}$, conserved because of the stable stratification. Assuming a selective decay during relaxation (the magnetic energy decays much faster than $\mathcal{H}$ and M_Ψ as observed by Braithwaite 2008, so that they can be considered constant on an energetic decay e-folding time), a variational method allows us to derive the elliptic linear partial differential equation governing Ψ (Woltjer 1959; Montgomery & Phillips 1989; Duez & Mathis 2010):

$$\Delta^*\Psi + \frac{\lambda_1^2}{R^2}\Psi = -\mu_0\,\overline{\rho}\,r^2\sin^2\theta\,\beta_0. \quad (3)$$

Here, $\overline{\rho}$ is the density in the non-magnetic case, $\Delta^*\Psi \equiv \partial_{rr}\Psi + \sin\theta\,\partial_\theta\left(\partial_\theta\Psi/\sin\theta\right)/r^2$ is the Grad–Shafranov operator in spherical coordinates, λ_1 is a coefficient to be determined, R is a characteristic radius, and β_0 is constrained by the field's intensity. This equation is similar to the Grad–Shafranov equation used to find equilibria in magnetically confined plasmas (Grad & Rubin 1958; Shafranov 1966), the source term being here related to the stellar structure through $\overline{\rho}$ (see Heinemann & Olbert 1978 for a discussion of the general form of this equation in astrophysics). Furthermore, this equilibrium is in a barotropic state (in the hydrodynamic meaning of the term, i.e., isobar and iso-density surfaces coincide), where the field is explicitly coupled with stellar structure through $\boldsymbol{\nabla}\times(\boldsymbol{F}_{\mathcal{L}}/\overline{\rho}) = \mathbf{0}$, where $\boldsymbol{F}_{\mathcal{L}}$ is the Lorentz force. This is a generalization of Prendergast's equilibrium taking into account compressibility, first studied in polytropic cases by Woltjer (1960).

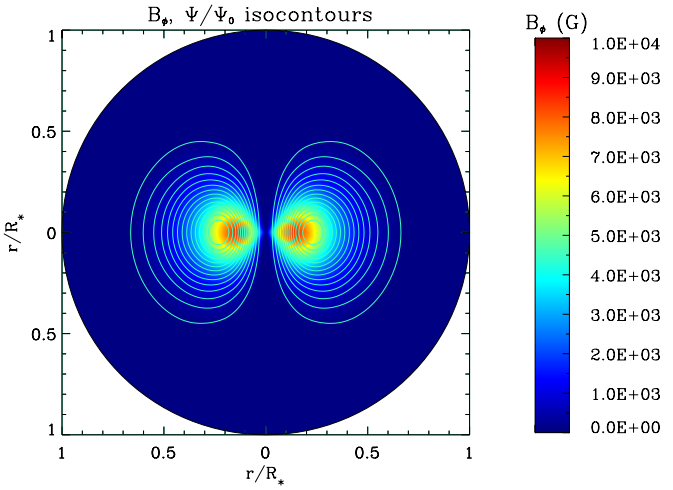

Figure 1. Toroidal magnetic field strength in colorscale (arbitrary field's strength) and normalized isocontours of the poloidal flux function Ψ in meridional cut for the first equilibrium configuration ($\lambda_1^1 \simeq 33$). The neutral line is located at $r \simeq 0.23\,R_*$.

2.2.2. Solution

We now discuss the boundary conditions. In Duez et al. (2010) and Duez & Mathis (2010), we considered the general case of a field confined between two radii, owing to the possible presence of both a convective core and a convective envelope and to ensure the conservation of magnetic helicity. We here choose to cancel both radial and latitudinal fields at the surface, to avoid any current sheets, conserving once again magnetic helicity. Owing to its small extension, the possible effects of the convective core on the large-scale surrounding field are neglected. Using Green's function method, we finally obtain the purely dipolar, general solutions indexed by i:

$$\Psi_i(r,\theta) = -\mu_0\beta_0\frac{\lambda_1^i}{R}r\left\{j_1\left(\lambda_1^i\frac{r}{R}\right)\int_r^R\left[y_1\left(\lambda_1^i\frac{\xi}{R}\right)\overline{\rho}\xi^3\right]d\xi + y_1\left(\lambda_1^i\frac{r}{R}\right)\int_0^r\left[j_1\left(\lambda_1^i\frac{\xi}{R}\right)\overline{\rho}\xi^3\right]d\xi\right\}\sin^2\theta, \quad (4)$$

R being the upper boundary confining the magnetic field; λ_1^i are the set of eigenvalues indexed by i allowing to verify the boundary conditions. The functions j_l and y_l are, respectively, the spherical Bessel functions of the first and the second kind. As shown in Duez & Mathis (2010), the first radial mode is the lowest energy state. We thus focus here only on this mode $i = 1$. The toroidal magnetic field is then given using $F(\Psi) = \lambda_1\Psi/R$; in the case of a stably stratified $n = 3$ polytrope and for the simulation purposes where we set $R = 0.85\,R_*$, we have $\lambda_1 \simeq 32.95$, while for a constant density profile (in a zero gravity medium), we have $\lambda_1 \simeq 5.76$. The solution for the $n = 3$ polytrope is represented in Figure 1. The ratio of the poloidal to total magnetic energy density $B_{\rm p}^2/B^2\,(r,\theta)$ is plotted as a function of the radius in Figure 2, for various latitudes. Note that its integrated value $E_{\rm p}/E \simeq 5.2\times10^{-2}$ is in the range of ratios found in stable axisymmetric equilibria forming in simulations from random small-scale initial conditions (Braithwaite & Nordlund 2006).

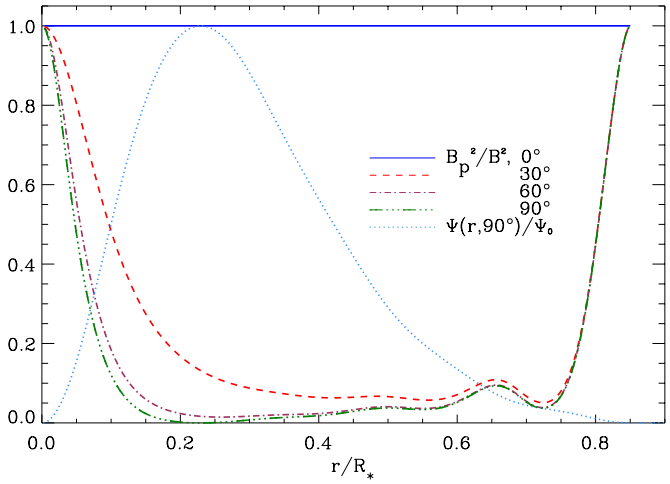

Figure 2. Poloidal to total magnetic energy density B_p^2/B^2 as a function of the radius for different colatitudes and radial profile of the poloidal flux function Ψ at the equator.

3. STABILITY: NUMERICAL METHOD

3.1. The Numerical Model

The setup of the numerical model is similar to that in Braithwaite & Nordlund (2006), where a fuller account can be found; a brief outline is given here. We use the Stagger code (Nordlund & Galsgaard 1995), a high-order finite-difference Cartesian MHD code containing a "hyper-diffusion" scheme. We use a resolution of 192^3.

We model the star as a self-gravitating ball of ideal gas ($\gamma = 5/3$) with radial density and pressure profiles initially obeying the polytropic (thus barotropic) relation $P \propto \rho^{1+(1/n)}$, with index $n = 3$—a good approximation to an upper-main-sequence star. It seems unlikely that a different equation of state, for instance that of a neutron star, will make even much quantitative difference to the results. The important point is the stable stratification.

We use this model to compare the dynamical evolution of the mixed (poloidal–toroidal) configuration to that of its purely poloidal and toroidal components on their own, both of which are unstable as mentioned above. We should therefore see these instabilities, growing on an Alfvén timescale. To test the stability of the configurations, we add a random "white noise" perturbation to the density field. The perturbation (1% in amplitude) contains length scales ranging from R_* to 0.08 R_*, the latter being double the Nyquist wavelength. This is roughly equivalent to azimuthal wavenumbers up to $m = 38$ at a radius of $R_*/2$.

3.2. Results

Purely poloidal component. The simulation is run for around 10 Alfvén crossing times τ_A, over which time the instability grows, becomes non-linear, and results in the destruction of most of the original magnetic energy. The magnetic field amplitude is plotted at the top left of Figure 3, split into components according to azimuthal wavenumber m; obviously at $t = 0$ all the energy is in the axisymmetric $m = 0$ part. The bottom-left plate of the figure shows the mean velocity in each azimuthal mode. Note the clear transition at $t \approx 2\,\tau_A$ from the linear phase to the non-linear, reconnective phase.

Purely toroidal component. The middle plates of Figure 3 show the evolution of the toroidal field—clearly, the $m = 1$ mode is dominant. In the lower panel of Figure 4 are drawn the magnetic field lines for the evolved configuration, i.e., at $t \approx 10\,\tau_A$. After the linear growth of the $m = 1$ mode, the Tayler instability manifests itself in the non-linear regime (cf. Brun 2007; Elstner et al. 2008). We find here that although the linear stability conditions are local in the θ direction, the non-linear displacement field is global in that direction: as can be seen in Figure 4 we have essentially a motion of spherical shells relative to one another. We expect eventual complete destruction of the field on a longer timescale; however, a more detailed investigation is left to a forthcoming paper.

Mixed configuration. The mixed poloidal–toroidal configuration exhibits completely different behavior. The magnetic and velocity amplitudes are plotted on the right of Figure 3, where

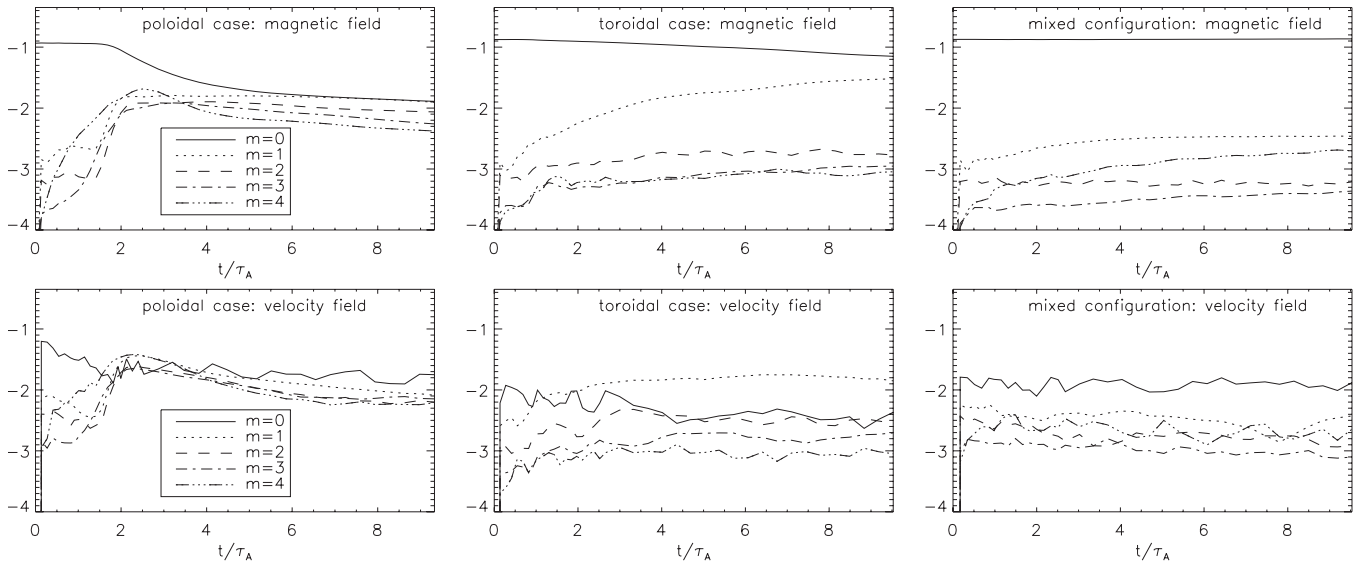

Figure 3. Time evolution of the (log) amplitudes in azimuthal modes $m = 0$–4 averaged over the stellar volume of the magnetic field (top row) and the velocity field (bottom row) in the simulations with the purely poloidal field (left), purely toroidal field (middle), and the mixed field (right). Initially, all the magnetic energy is in the $m = 0$ mode since the initial conditions are axisymmetric.

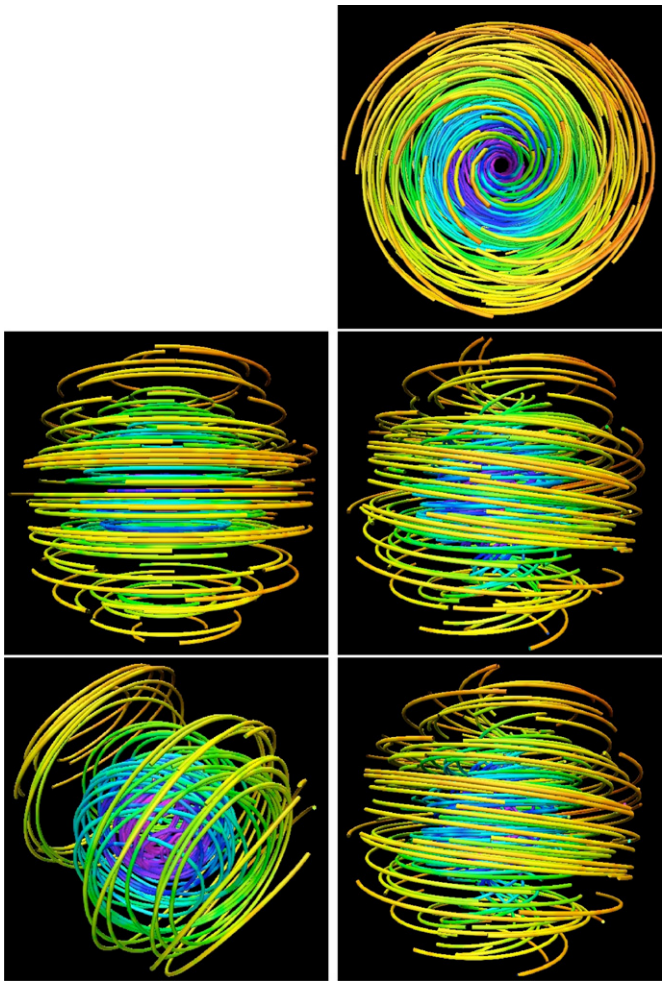

Figure 4. Snapshots from simulations representing magnetic field lines (the colorscale is a function of the density). Left-hand panels: purely toroidal component; right-hand panels: the mixed field configuration. Upper and middle panels: configurations at $t = 0$; lower panels: configuration at $t = 10\ \tau_A$. The upper-right panel shows the field from a different perspective, looking down the axis.

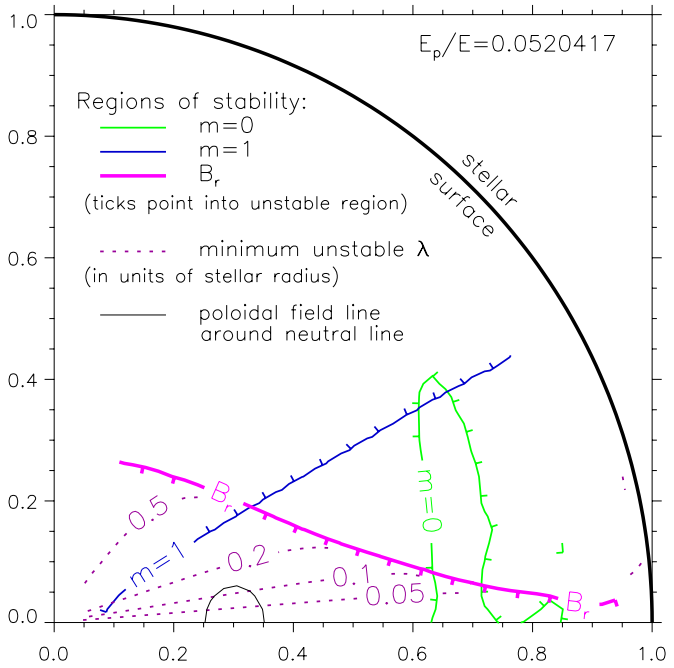

Figure 5. Half of the meridional plane, showing the regions stable against the $m = 0$ and 1 Tayler modes in the absence of the poloidal component and their stabilization by the radial component B_r.

we see an absence of growing modes. The kinetic energy present results simply from the initial perturbation and the oscillations and waves it sets up. In Figure 4 are drawn the magnetic field lines at $t = 0$ and 10 τ_A; no significant change is seen.

To better examine the potentially unstable regions, we use Tayler's stability criteria (Tayler 1973) for purely toroidal fields and estimate the stabilization from the poloidal component, following Braithwaite (2009). In Figure 5, we plot Tayler's criteria for modes $m = 0$ and $m = 1$—the $m = 0$ mode is unstable almost everywhere and the $m = 1$ mode is unstable in a large cone around the poles; however, the poloidal field stabilizes these modes in most of the meridional plane except near the equatorial plane where it merely stabilizes all wavelengths small enough to fit into the available space. Moreover, we can examine closely the behavior of the field in the vicinity of the magnetic axis, where it can be approximated as the addition of an axial and a toroidal field (cylindrical geometry). Bonanno & Urpin (2008a) outlined that in this case magnetic configurations can be subject to non-axisymmetric resonant instability. They determined the dependency of the Tayler's instability maximum growth rate as a function of the azimuthal wavenumber m and of the ratio ε of the axial field to the toroidal one. In our case, close to the center the flux function exhibits a behavior in $\Psi \propto r^2$, so the azimuthal field is proportional to $s = r \sin\theta$ corresponding to the Bonanno et al.'s parameter $\alpha = 1$. As underlined by the authors, in that case the maximum growth rate changes remarkably slowly with m for all modes with $m \geqslant 2$, and the instability is weakly non-anisotropic. If we take as a value for s_1 the radius of the neutral line or the one where the azimuthal field is strongest, we obtain, respectively, $\varepsilon = 0.64$ or $\varepsilon = 0.79$. According to their study (see Bonanno & Urpin 2008a, Figure 7), we fulfill the stability criterion for the modes $m = 0$, 1, and 2. Our results are therefore in agreement with their linear analysis.

In the simulations we run, the mixed configuration has a poloidal energy fraction $E_p/E = 0.052$. The magnetic-to-thermal energy ratio $E/U \approx 1/400$, which should mean that for stability we require $E_p/E \gtrsim 0.04$ (Braithwaite 2009). We see then that this value of E/U is near the upper limit for stability—in other words, we are near the boundary of validity of the weak-field approximation used in Section 2.

4. CONCLUSION

Using semi-analytic methods, we derived (with an appropriate choice of boundary conditions) and then tested an axisymmetric non-force-free magnetostatic equilibrium which could exist in any non-convective stellar region: the radiative core of solar-type stars, the external envelope of massive stars, and compact objects. Using numerical simulations, we demonstrate the ability of the setup to recover well-known instabilities in purely poloidal and toroidal cases, and then find stability of the mixed configuration under all imaginable perturbations. We show the agreement of the result with linear analysis (limited in perturbations), highlighting the stabilizing influence of the poloidal field on the toroidal one, especially in the region close to the symmetry axis where purely toroidal fields usually develop kink-type instabilities in priority. This is the first time the stability of an analytically derived stellar magnetic equilibrium has been confirmed numerically. This result has strong

astrophysical implications: the configuration, as described in Duez & Mathis (2010), provides a good initial condition to magnetohydrodynamic simulations and magneto-rotational transport to be included in next-generation stellar evolution codes—where up to now the initial field would have been chosen arbitrarily; furthermore, it will help us to appreciate the internal magnetic structure of neutron stars and various astrophysical processes involving magnetars (intense activity in the X-ray and gamma-ray spectra, quasi-periodic oscillations, and eventually gamma-ray bursts).

The authors thank N. Langer, Å. Nordlund, J.-P. Zahn, A.-S. Brun, and the MIMES collaboration for fruitful discussions and assistance. We are grateful to the anonymous referee for providing comments that helped improve the manuscript. This work was supported in part by the French PNPS (CNRS/INSU).

REFERENCES

Alecian, E., et al. 2008, Contributions of the Astronomical Observatory Skalnaté Pleso, 38, 235
Aurière, M., et al. 2007, A&A, 475, 1053
Bonanno, A., & Urpin, V. 2008a, A&A, 488, 1
Bonanno, A., & Urpin, V. 2008b, A&A, 477, 35
Braithwaite, J. 2006, A&A, 449, 451
Braithwaite, J. 2008, MNRAS, 386, 1947
Braithwaite, J. 2009, MNRAS, 397, 763
Braithwaite, J., & Nordlund, Å. 2006, A&A, 450, 1077
Braithwaite, J., & Spruit, H. C. 2004, Nature, 431, 819
Brun, A. S. 2007, Astron. Nachr., 328, 1137
Busse, F. H. 1981, Geophys. Astrophys. Fluid Dyn., 17, 215
Commerçon, B., Hennebelle, P., Audit, E., Chabrier, G., & Teyssier, R. 2010, A&A, 510, L3
Decressin, T., Mathis, S., Palacios, A., Siess, L., Talon, S., Charbonnel, C., & Zahn, J.-P. 2009, A&A, 495, 271
Duez, V., & Mathis, S. 2010, A&A, 517, A58
Duez, V., Mathis, S., & Turck-Chièze, S. 2010, MNRAS, 402, 271
Eff-Darwich, A., Korzennik, S. G., Jiménez-Reyes, S. J., & García, R. A. 2008, ApJ, 679, 1636
Elstner, D., Bonanno, A., & Rüdiger, G. 2008, Astron. Nachr., 329, 717
Grad, H., & Rubin, H. 1958, in Proc. 2nd UN Int. Conf. on the Peaceful Uses of Atomic Energy, Vol. 31, IAEA (Geneva: UN), 190
Grunhut, J. H., et al. 2009, MNRAS, 400, L94
Heinemann, M., & Olbert, S. 1978, J. Geophys. Res., 83, 2457
Mathis, S., & Zahn, J.-P. 2005, A&A, 440, 653
Montgomery, D., & Phillips, L. 1988, Phys. Rev. A, 38, 2953
Montgomery, D., & Phillips, L. 1989, Physica D, 37, 215
Nordlund, Å., & Galsgaard, K. 1995, A 3D MHD code for Parallel Computers, http://www.astro.ku.dk/~aake/papers/95.ps.gz
Prendergast, K. H. 1956, ApJ, 123, 498
Reisenegger, A. 2009, A&A, 499, 557
Shafranov, V. D. 1966, Rev. Plasma Phys., 2, 103
Shaikh, D., Dasgupta, B., Hu, Q., & Zank, G. P. 2008, J. Plasma Phys., 75, 107
Tayler, R. J. 1973, MNRAS, 161, 365
Taylor, J. B. 1974, Phys. Rev. Lett., 33, 1139
Woltjer, L. 1959, ApJ, 130, 405
Woltjer, L. 1960, ApJ, 131, 227
Wright, G. A. E. 1973, MNRAS, 162, 339
Zahn, J.-P. 1992, A&A, 265, 115